ELSEVIER SAUNDERS

POSITRON EMISSION TOMOGRAPHY

PET Clin 2 (2007) 251–266

Strategies for Motion Tracking and Correction in PET

Arman Rahmim, PhD[a,*], Olivier Rousset, PhD, PD[a], Habib Zaidi, PhD[b]

Recent developments in three-dimensional (3D) PET systems have enabled the spatial resolution to reach the 2- to 5-mm full-width-at-half-maximum (FWHM) range [1]. With such improvements in spatial resolution, even small amounts of motion during PET imaging become a significant source of resolution degradation. In other words, increased spending on new-generation scanners can be fully justified only when appropriate motion correction methods are considered, to achieve the true resolution of the scanner [2]. To demonstrate, the effective resolution of an image $FWHM_{eff}$ can be written as

$$\mathrm{FWHM}_{\mathrm{eff}} = \sqrt{\mathrm{FWHM}^2_{\mathrm{tomograph}} + \mathrm{FWHM}^2_{\mathrm{motion}}} \qquad (1)$$

where $FWHM_{tomograph}$ denotes the intrinsic resolution of the scanner and $FWHM_{motion}$ is the FWHM of the distribution of the patient's motion. With $\mathrm{FWHM}_{\mathrm{tomograph}}$ having become comparable to (and no longer much larger than) $\mathrm{FWHM}_{\mathrm{motion}}$, it is therefore essential to develop and implement accurate patient motion correction techniques.

Motion correction methods developed for single-photon emission CT (SPECT) are not necessarily applicable to PET because thethey may rely on the time-dependence of projections in SPECT (due to a rotating head or heads), which is not the case in PET. Nevertheless, a number of other methods implemented in SPECT are equally applicable to PET (and vice versa) and are reviewed in this work. This article has been broadly categorized into the review and discussion of advanced correction methods for the cases of unwanted patient motion, motion due to cardiac cycles, and motion due to respiratory cycles. Most of the existing literature on the first type of motion has been investigated and implemented in brain PET imaging because the last two types of motion (which are dominant in whole-body and cardiac PET imaging) are absent

This work was supported by grant SNSF 3100A0-116547 from the Swiss National Foundation.
[a] Division of Nuclear Medicine, Russell H. Morgan Department of Radiology and Radiologic Sciences, Johns Hopkins University, Room 3245, 601 N. Caroline Street, Baltimore, MD 21287, USA
[b] Division of Nuclear Medicine, Geneva University Hospital, CH-1211, Geneva, Switzerland
* Corresponding author.
E-mail address: arahmim1@jhmi.edu (A. Rahmim).

1556-8598/07/$ – see front matter
doi:10.1016/j.cpet.2007.08.002
pet.theclinics.com

in this case. Therefore, the first section discusses motion correction methods in brain PET imaging and the next two sections include an overview of advanced correction methods for cardiac and respiratory cycle motions, respectively. These sections discuss existing hardware instrumentation and review advanced motion correction algorithms that make use of such hardware to achieve motion-compensated PET images. Lastly, some important areas of future research are discussed.

Brain PET imaging

Unlike cardiac- and respiratory-related motions, patient movements in brain imaging are assumed to be of rigid nature (ie, modeled as translational and rotational transformations only). Because a typical PET brain imaging session can last hours, it is not reasonable to expect a patient to remain motionless during this time [3]. A number of head restraints are common nowadays, such as thermoplastic masks or neoprene caps that lower the amount of motion but do not eliminate it [4]. Even with head restraints, typical translations in the range of 5 to 20 mm and rotations of 1° to 4° are observed[1], depending on the type of mask and the duration of scan (eg, see Refs. [5,6] and Ref. [2] in which a study of various types of head movement, such as those caused by coughing and leg crossing, has been presented).

Methods to correct for such patient movements were in the past largely based on correction of inter-scan movements [7]. These (software-based) methods typically involve the division of a scan into a number of frames, followed by spatial registration of the reconstructed images using mathematical algorithms (eg, see Refs. [8–10]). Alternatively, hybrid motion estimation/correction methods have been proposed [11,12] that use forward-projected data to detect brain motions and incorporate this information into 3D iterative reconstructions. Nevertheless, motion correction strategies in emission CT (ECT) that rely exclusively on emission data are likely inadequate for robust clinical usage because they (1) depend on the quality of the scan data, including noise characteristics; and (2) assume that the activity distribution does not change significantly within the frames, whereas the frames are chosen a priori [13]. Because of these disadvantages, this review focuses on methods that use external real-time measurements of motion.

Instrumentation

Aside from electromagnetic systems (which suffer from interference with eddy currents in the metal within the PET gantry) and acoustical devices (whose audible signal can be unacceptable especially for neurologic studies), the following motion-tracking instruments have been used by many groups:

1. A video camera–based surveillance system by Picard and Thompson [14] uses three LEDs attached to the head of the patient. The system has two charge-coupled device cameras placed on the gantry of the PET scanner.
2. The system by Goldstein and colleagues [15] is based on optoelectronic position sensitive detectors and uses an optical triangulation of three miniature (lamp) lights fixed to the patient's head. The large space between the cameras (1.25 m), however, prevents the use of this system in PET scanners that have long and narrow gantry holes.
3. The currently popular high-resolution (<0.3 mm) POLARIS system [2] is an infrared (IR) optoelectronic motion-tracking device that uses four IR-reflective spheres (Fig. 1). The advantages of the system are that it is commercially available (<$15,000; Northern Digital Inc., Waterloo, Canada) and uses IR light[2], so it is insensitive to room lighting conditions and takes much less disk space to store the IR-tracker output compared with optical image sequences. The disadvantages of POLARIS it that it has reflective spheres that need to be affixed in a precisely known geometry and, similar to all aforementioned methods, the issue of possible relative

Fig. 1. The POLARIS system uses four IR-reflective spheres placed in a precisely known geometry. (*Courtesy of* Northern Digital Inc., Waterloo, Canada; with permission.)

[1] The largest translation typically occurs along the transaxial-(x) axis, and the largest rotation around the axial-(z) axis.

[2] A system with charge-coupled device video cameras also sensitive to IR light was used by Menke and colleagues [16]; however, the reflectors were affixed to a landmark device that was rigidly attached to the teeth of the subject's upper jaw, which proved to be inconvenient for the patients.

motion between the skin and the skull during the scan remains potentially problematic, making the accuracy of these techniques questionable. It is a topic of growing and great interest to the ECT community to minimize or eliminate the latter problem through innovative methods and technology.

Motion-correction algorithms

Assuming accurate measurement of patient movement during the scan, a number of approaches to motion compensation have been proposed.

One method [5,14] involves dividing detected events into multiple acquisition frames (MAFs). With the use of an external monitoring system, every time the displacement of the patient is measured to be larger than a specified threshold, the PET data are saved in a new frame. This step is then followed by correction of the individually reconstructed images of the MAFs by way of rotation and translation, to compensate for the measured amount of motion (ie, an image-driven approach).

The major limitation of the MAF approach is that by using a high motion threshold, motion within the frames is neglected; lowering the motion threshold can result in the acquisition of an increasing number of low-statistic frames to be reconstructed, especially in the presence of considerable movement [3]. Lack of an adequate number of acquired events in the individual frames can, in turn, adversely affect the quality of the final reconstructed images; an increased number of frames leads to increased reconstruction times.

An image-driven correction method proposed by Menke and colleagues [16] involves postprocessing of the motion-blurred reconstructed images using deconvolution operators (whose shape is determined by the measured motion). The technique was later further refined by combining patient-specific motion estimates of tissue trajectories with image deconvolution techniques [17]. Nevertheless, this method has not attracted much attention because even though it is theoretically accurate for noiseless data, the deconvolution process amplifies the noise in the PET data, and when the movements include significant rotation, spatially variant deconvolution filters need to be employed, which increases the computational costs and can introduce other artifacts [16].

Another possible approach is to model the effect of motion in (the image-space component of) the system matrix of the expectation maximization (EM) algorithm. This approach can be powerful (eg, see Refs. [18–21]) for compensating cardiac and respiratory motion, in which assumptions of rigid motion are violated (this is further elaborated in later sections). In the context of nongated motion-contaminated (brain imaging) data, the approach has been used to incorporate the overall externally tracked motion into the reconstruction task [22]. This method, however, is not preferred for scanners that have the capability to compensate individually detected events for motion (described next) because it merely models the overall motion of the subject and would converge very slowly.

A more accurate approach consists of correcting individual lines of response (LORs) for motion [23] (ie, an event-driven approach). Motion correction is performed by transforming the LORs along which the events are measured to where they would have been measured if the object had not moved, as shown in Fig. 2 for the example of an octagonal PET scanner.

The method was elaborated and implemented by Menke and colleagues [16] and required some hardware modification to achieve on-the-fly motion-corrected LORs. In that work, due to hardware limitations, the corrected LORs where not corrected by normalization factors that corresponded to the original detector pairs (along which the events were detected); instead, the normalization factors for the transformed LORs were used. This normalization mismatch has recently been shown to result in artifacts [24].

To solve this problem, one requires a PET scanner equipped with more specialized hardware to achieve accurate on-the-fly normalization correction followed by LOR-transformation [25] or a PET scanner capable of acquiring data in list-mode format so that LOR corrections can be accurately performed post acquisition [6].

Beyond the purely event-driven approach

The event-driven approach neglects two issues [26,27].

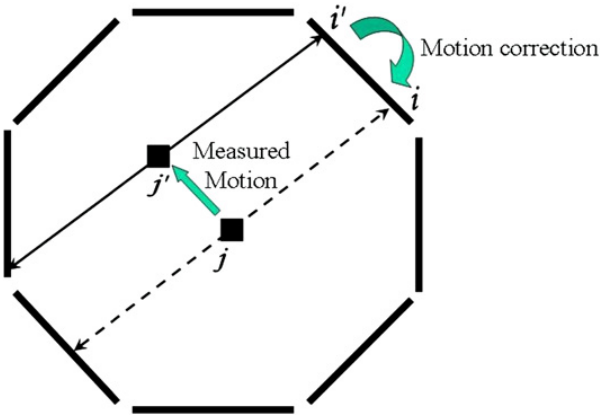

Fig. 2. An event that would have been generated at position j and detected along LOR_i is instead generated at position j' and detected along $LOR_{i'}$ because of motion. From the measured motion information, one can then transform $LOR_{i'}$ back into LOR_i.

Issue 1 An event that is normally detected can exit the field of view (FoV) undetected because of motion, which results in a loss of events that would normally have been detected. This effect is not modeled by regular reconstruction methods.

Issue 2 Alternately, an event that is normally not detected (ie, not in the FoV) may be detected because of motion. Therefore, after correction for motion, some detected events may correspond to no actual detector pairs.

These two effects can occur in two ways: (1) along the axial direction of the scanner, by way of translation (Fig. 3) or rotation (not shown); or (2) similarly by way of translation or rotation along the transaxial direction, but only for scanners that have gaps between the detectors (an example is the high-resolution research tomograph [HRRT] [28], which has an octagonal design with gaps between the heads, or the hybrid photon detectors–based brain PET with long axially oriented scintillator crystals [29]). This effect is shown in Fig. 4 for the HRRT (for the case of translation).

The presence of these two issues can imply the need for a more accurate modeling of the image–data relation into the reconstruction task; otherwise, neglecting the first issue can produce image artifacts, as demonstrated by simulations [24,30] or experimental measurements [27], and neglecting the LORs obtained in the second case can result in a decrease of signal-to-noise ratio (SNR) in the resulting images. A number of proposed solutions to one or both of these issues are reviewed in the following paragraphs.

A method suggested by Thielemans and colleagues [30] addressing issue 1 involves scaling the counts recorded in the motion-corrected sinogram bins to correct for the events that were lost due to motion. The scale factors are computed by

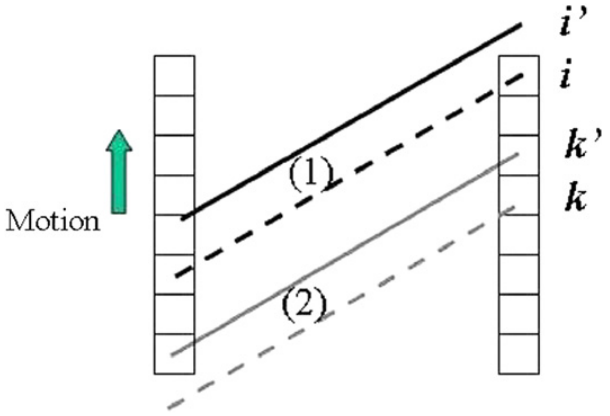

Fig. 3. Axial motion can result in LOR_i not to be detected (i') [issue (1)] and LOR_k, which is normally not detected, to actually be detected (as LOR_k) [issue (2)]. The effect shown is due to translation but is equally valid for rotation.

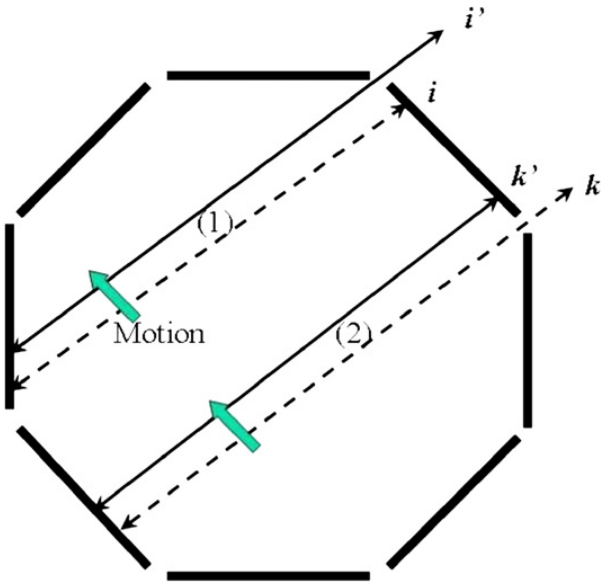

Fig. 4. Transaxial motion, for scanners with gaps between the detector heads, can result in the same issues shown in Fig. 3.

averaging LOR weighting factors using the measured motion information. This method can be thought of as a "motion precorrection" technique applied to the sinogram bins before the image reconstruction task.

The method investigated by Bühler and colleagues [24], similarly addressing issue 1, involves using the motion information to divide the total counts in each motion-corrected sinogram bin by the factor $t_{detectable}/t_{total}$ (ie, the fraction of time each sinogram bin could have been detected by the scanner). Aside from the issue of normalization correction, this method can be shown (although it is not obvious) to be equivalent to the previous method; however, this method precorrects the individual measured events by related normalization factors, whereas the previous method, which is expected to exhibit less noise [30], first sums the non-normalized motion-corrected LORs and then performs normalization correction (by an accurately calculated overall factor).

These two methods have two potential difficulties: (1) they may require consideration of noise enhancement issues, as is done by Thielemans and colleagues [30] when dividing by small-scale factors; and (2) they address issue 1 but not issue 2 because they simply discard motion-corrected events that do not correspond to actual detector elements. It must be noted that neglecting such events should not result in image artifacts (unlike neglecting issue 1) because the patient will be still sampled enough by the existing detector pairs; however, it can result in a reduced SNR in the images because part of the measured signal with useful information is simply discarded.

In a comprehensive solution, Qi and Huesman [31] proposed a reconstruction approach that addressed both aforementioned issues by way of modification of the probability system matrix of the iterative EM algorithm. Momentarily neglecting various correction terms (eg, normalization, attenuation), the regular EM algorithm can be written (working in histogram-mode) as

$$f^{\text{new}}(j) = \frac{f^{\text{old}}(j)}{\sum_{i=1}^{I} p_{ij}} \sum_{i=1}^{I} \frac{p_{ij} n(i)}{\sum_{j=1}^{J} p_{ij} f^{\text{old}}(j)} \tag{2}$$

where $f^{\text{old}}(j)$and $f^{\text{new}}(j)$are previous and current activity distribution image estimates in the iterative EM algorithm, $n(i)$ is the number of events detected along an LOR i, and p_{ij}, often referred to as the system matrix, is the probability that an emission from voxel j ($j = 1 \ldots J$) is detected along an LOR i ($i = 1 \ldots I$). For a motion-corrected sinogram (wherein all the events were first corrected for motion before histogramming), the proposed algorithm is able to accurately address issues 1 and 2, and can be written as

$$f^{\text{new}}(j) = \frac{f^{\text{old}}(j)}{\frac{1}{T}\int_{t=0}^{T} \sum_{i=1}^{I} p_{ij} \delta_i^t \mathrm{d}t} \sum_{i=1}^{I} \frac{p_{ij} n(i)}{\sum_{j=1}^{J} p_{ij} f^{\text{old}}(j)} \tag{3}$$

where T is the duration of the scan and δ_i^t is 1 if an LOR i is in the FoV at time t and is 0 otherwise. Normalization correction can subsequently be included as a precorrection factor (similar to Ref. [24]) or as an intrinsic component of the system matrix element. The reader is referred to Rahmim and colleagues [32] for more details.

This approach has also been implemented [27,31,32] for list-mode image reconstruction. The list-mode reconstruction approach has a number of general advantages compared with the histogram-mode approach [33,34] in the context of motion correction.

Events are corrected for motion during (and not before) the image reconstruction task, which means that the motion-corrected coordinates can be processed as continuous variables, therefore potentially improving the accuracy. Histogram-mode methods [24] may require time-consuming interpolations because sinogram bins are not continuous.

Addressing issue 2 is more convenient in list-mode reconstruction, because in histogram-mode methods, one would have to extend the sinogram-space to record all motion-corrected events, even those that would not have been detected in the absence of motion. In list-mode reconstruction, such events are very easily handled.

Furthermore, Rahmim and colleagues [27] have also shown that with appropriate modifications, calculation of the motion-averaging term $\frac{1}{T}\int_{t=0}^{T} \sum_{i=1}^{I} p_{ij} \delta_i^t \mathrm{d}t$ can be conveniently and accurately performed in image-space (instead of projection-space). The result for current high-resolution scanners is that the calculation speed can be improved significantly (eg, the HRRT scanner, with no axial compression [ie, span 1], has ~800 M sinogram bins compared with only ~14 M voxels in image-space). In projection-space, Carson and colleagues [35] have proposed to perform the previous calculation over a randomized subset of the projection-space only, to produce a fast, practical algorithm. It has been shown, however, that the particular randomization method is critical to the accuracy of the estimated sensitivity factors [36], particularly because inaccuracies are amplified in subsequent iterations of the EM algorithm. More accurate (yet more time-consuming) Monte Carlo randomization techniques have been proposed [37].

Motion due to the cardiac cycle

Although a spatial resolution of less than 5 mm is possible with current-generation PET scanners, the base of the heart moves 9 to 14 mm toward the apex, and the myocardial walls thicken from approximately 10 mm to over 15 mm between end-diastole and end-systole, as measured from tagged MR images [38]. Compared with the intrinsic resolution of today's scanners, cardiac motion can therefore result in significantly blurred images (Equation 1). The most common approach to cardiac cycle motions in ECT is gating of the data into frames, with each frame representing a particular cardiac phase.

Instrumentation

Gating of the cardiac cycle is most commonly performed with the aid of ECG devices. By convention, the R wave (which precedes ventricular contraction) is chosen as the gating signal because it has the greatest amplitude and is therefore more easily identified on the ECG. In scanners equipped with list-mode acquisition capability, sorting of the list-mode data into gated frames can be performed after the acquisition [39–42], whereas in conventional scanners (ie, with histogram-mode acquisition only), on-the-fly ECG-triggered data acquisition is employed [43,44].

Typically, the cardiac cycle is divided into 50- to 100-millisecond time frames, and an acquisition ranging from 5 to 60 minutes is usually acquired. Most commonly, the obtained cardiac-gated datasets (ie, cardiac frames) are independently reconstructed (Fig. 5). This approach is successful in

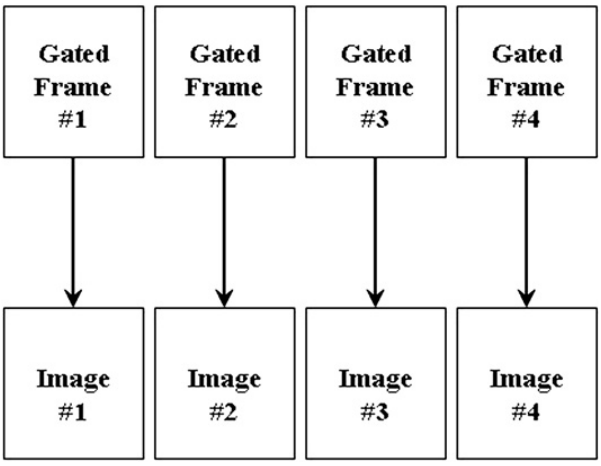

Fig. 5. In conventional gated schemes, the gated frames are independently reconstructed (in this example, N = 4 gated frames are shown).

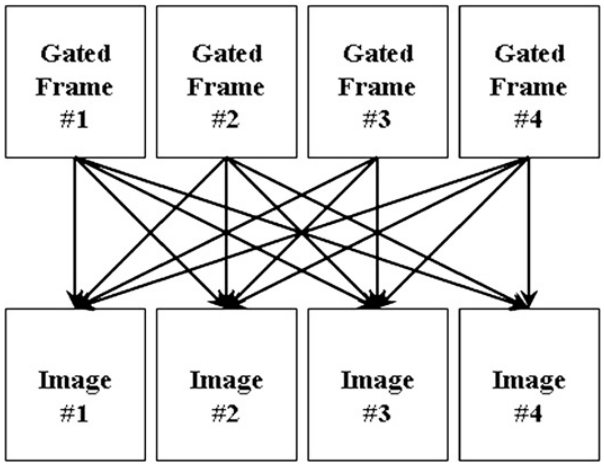

Fig. 6. In motion-correction gated schemes, individual images are reconstructed using information from the complete dataset.

nearly removing the cardiac-motion blurring of the images; however, it usually produces images that are much noisier than a reconstruction of the ungated data because each gated dataset contains less statistics than the entire dataset. The clinical utility of this approach is therefore questionable.

Motion-correction algorithms

The motivation behind advanced correction methods in cardiac imaging is twofold. First, advanced correction methods improve the quality of cardiac PET images (noise, resolution) to enhance the identifiability of radiotracer uptake defects in the left ventricle by clinicians, because regions of decreased radiotracer uptake can be indicative of hibernating or infracted myocardial tissue [45]. Motion correction is also important when applying quantitative measures of perfusion and metabolic parameters in dynamic compartmental modeling studies [46]. Second, the measurement of motion itself can be useful for characterizing cardiac function [47]. Measures such as ejection fraction and regional wall thickening may be derived from a measure of contractile motion in this way.

The problem of cardiac motion due to the respiratory cycle is discussed in a later section [48,49]. In this section, the authors review a variety of motion correction approaches that have been proposed in the literature. A common theme among these advanced methods is that they seek to move beyond the conventional gated scheme (see Fig. 5) and instead seek to obtain images of higher quality by making collective use of all the gated frames (Fig. 6).

Broadly, three types of general approaches were reported in the literature: (1) nonrigid registration of independently reconstructed images; (2) initial estimation of the motion information from the gated PET or CT images, which is subsequently used in a new reconstruction applied to all the gated frames; and (3) simultaneous estimation of the motion parameters and the images. Asma and colleagues [50] theoretically analyzed and compared the first and second general approaches and showed that the latter was better suited to produce images of higher quality (similar bias, improved noise) for standard EM and penalized likelihood algorithms (in which a high degree of smoothing is not used). A thorough comparison (using analytic, Monte Carlo simulation, and experimental studies) between the second and third approach remains to be performed.

The following summarizes the approaches taken within the aforementioned three categories:

Category 1

Klein and Huesman [51] developed a sophisticated motion-estimation approach making use of a nonuniform elastic-material model to provide accurate estimates of heart motion (from individually reconstructed gated frames). These investigators continued to perform nonrigid/deformed summing of the gated images using the motion information (ie, image-driven motion compensation).

Dawood and colleagues [13,52] combined the acquisition of gated PET data with optical flow techniques to calculate motion vector and to correct for it using nonlinear registration techniques. A similar approach, referred to as "retrospective stacking," was used to reduce respiratory motion artifacts in oncologic imaging [53]. These investigators reported improvements in contrast-to-noise ratios up to threefold over gated images and up to fivefold over ungated data.

Category 2

Brankov and colleagues [54,55] replaced the uniform-voxel framework with the use of mesh modeling: an efficient image description based on

nonuniform sampling (mesh nodes are placed most densely in image regions having fine detail). This approach is a natural framework for reconstruction of motion image sequences, wherein mesh elements are allowed to deform over time[3]. Using a gradient-descent search algorithm applied to initial cardiac gated images, the investigators estimated the motion field vector $d_{k\to l}(x)$, mapping a mesh element x from the current frame k to another frame l. Next, the following motion-compensated temporal summation was used when reconstructing each frame k:

$$\hat{f}_k(\mathrm{x}) = \sum_{l=1}^{K} f_l(\mathrm{x} - \mathrm{d}_{k\to l}(\mathrm{x})) \tag{4}$$

where $f_l(\mathrm{x})$ is the image estimate for the l^{th} frame ($k = 1 \ldots K$). Equation 4 can be applied as an inter-iteration temporal filter in iterative reconstruction or as a postreconstruction filter. (Although not shown here, these investigators added another term to Equation 4 to account for brightening of the myocardium as it thickens due to the partial volume effect.)

This summation/filtering step is therefore able to improve the SNR obtained in the cardiac images because it also makes use of information from other frames when reconstructing a given frame k. It should be noted, however, that this filtering framework is ad hoc in nature; the following is a discussion of methods performing theoretic-based four-dimensional (4D) reconstructions.

First, the maximum a posteriori probability (MAP) image reconstruction approach (with application to 4D motion-compensated imaging) is briefly reviewed. A main drawback with the commonly used EM algorithms is that with further iterations, the images become increasingly noisy [56]. As a solution, MAP-based methods[4] have been proposed that, in the 3D framework, seek to minimize variations between voxels and their neighboring voxels. Instead of maximizing the Poisson log-likelihood function $L(F)$, as is the case with the regular EM algorithm, a particular class of MAP methods (first used in nuclear medicine by Geman and McClure [57]) seeks to maximize the MAP function $L(F) - bV(F)$, where $V(F)$ is a potential function that decreases in value with less variations for neighboring voxels (b is a smoothing parameter set by the user: the higher its value, the greater the amount of smoothing encouraged in the images).

For instance, the so-called "3D-MAP-EM one-step-late" (OSL) algorithm, introduced by Green [58] and aimed to maximize the aforementioned MAP function, can be written as

$$f^{\mathrm{new}}(j) = \frac{f^{\mathrm{old}}(j)}{\sum_{i=1}^{I} p_{\mathrm{ij}} + \beta \left.\frac{\partial V(F)}{\partial f_j}\right|_{F=F^{\mathrm{old}}}} \sum_{i=1}^{I} \frac{p_{\mathrm{ij}} n(i)}{\sum_{j=1}^{j} p_{\mathrm{ij}} f^{\mathrm{old}}(j)} \tag{5}$$

This algorithm is able to suppress noise more successfully than the regular EM algorithm, which can be thought of as a special case of the MAP method, with $b = 0$. An observation is that this approach can be extended to a 4D-MAP algorithm [59–61] in which one uses a summation of spatial $\beta_s V_s(F)$ and temporal $\beta_t V_t(F)$potential functions to encourage smoothing between neighboring voxels in the spatial and temporal directions. The following paragraphs explain how motion compensation has been incorporated within the 4D-MAP framework in some of the noted works.

Gravier and colleagues [60,61] initially reconstructed the gated frames using the fast filtered backprojection algorithm, followed by low-pass filtering to reduce the noise. They then used the optical flow approach developed by Horn and Schunck [62] to estimate the motion between the reconstructed images. Finally, they used the 4D-MAP-EM-OSL algorithm while defining

$$V_t(F) = \sum_{k=1}^{K} \sum_{j=1}^{J} \left[f_k(j) - \frac{1}{K-1} \sum_{\substack{l=1 \\ l \neq k}}^{K} f_{l\to k}(j) \right] \tag{6}$$

where $f_{l\to k}(j)$denotes the estimated image intensity (in frame l) at the location corresponding to voxel j of frame k (considering the motion). In this way, smoothing is encouraged between voxels in all the frame sequences while taking the motion of the voxels into consideration. One is therefore able to suppress the noise level that is normally obtained in gated frame images.

In the work of Lalush and colleagues [59], a similar 4D-MAP-EM-OSL approach was considered, except that motion was modeled and assumed to be known a priori (and not measured from initial gated images). The motion vectors are computed by modeling the left ventricular inner and outer walls as ellipsoids that undergo affine transformations (rotation, scaling, and translation) within each frame. The exact form of the potential function

[3] See http://www.ipl.iit.edu/brankov/MIC02_4D.htm for a dynamic demonstration of this method.

[4] This method is also referred to as the bayesian method (originally derived from a simple application of Bayes' rule to image reconstruction). It is also sometimes referred to as penalized likelihood image reconstruction.

is also different in this work. It must be noted, however, that these investigators did not observe a noticeable degradation when the motion information was simply not included in the 4D-MAP algorithm method (which may have been due to the limited resolution of their scanner).

The MAP-EM-OSL algorithm as derived by Green [58] is based on an approximation (and breaks down for large values of b). In addition, it is a nontrivial task to select the parameters associated with the prior/penalty term. These parameters, which play an important role in the image quality, are often selected through trial and error. Finally, it is important to note that the aforementioned methods treat the same moving object as different temporal reconstructions that are merely temporally correlated. Nevertheless, a more concrete approach would involve a truly 4D approach in which the estimated deformations are incorporated within a unified cost function to be optimized (for a single object). Such an approach has been proposed and investigated by Qiao and colleagues [18,20], Li and colleagues [19], and Lamare and colleagues [56], who also compared implementation methodologies. In this approach, the measured nonrigid motion (estimated from the gated images) is modeled in the image-space component of the system matrix of the EM algorithm, and as such, a truly 4D EM reconstruction algorithm is achieved. This approach is very promising due to its accurate and comprehensive modeling of the relation of a moving object to detected events. The method has also been generalized by Qiao and colleagues [18,20] to incorporate only motions within a user-defined region of interest.

Category 3

Very commonly in the literature, cardiac motion is estimated after reconstructions of gated frames. In the previously mentioned techniques, this extracted motion information is used in subsequent reconstructions to yield enhanced images (ie, improved SNRs). Cao and colleagues [63], however, hypothesized that given the close link between the image reconstruction and motion estimation steps, a simultaneous method of estimating the two would be better able to (1) reduce motion blur and compensate for poor SNRs, and (2) improve the accuracy of the estimated motion. Their proposed algorithm works by two-step minimization of a joint energy functional term (including image likelihood and motion matching terms). This work has also been extended by Gilland and colleagues [64] from a two-frame approach to the complete cardiac cycle.

The approach taken by Jacobson and Fessler [65,66] considers a parametric Poisson model for gated PET measurements involving the activity distribution as unknown and a set of deformation parameters describing the motion of the image throughout the scan (from gate to gate). By maximizing the log likelihood for this model, a technique referred to as joint estimation with deformation modeling allows one to determine image and deformation parameter estimates jointly from the full set of measured data. This technique estimates a single image and *N-1* deformations, whereas the method of Gilland and colleagues [64] estimates *N* images and *N-1* motion deformations, thus involving a larger number of unknowns. At the same time, the cost function used in the article by Gilland and colleagues [64] does not involve deformations in the log-likelihood term, thus potentially simplifying the optimization task. This trade-off remains to be elaborately studied.

Motion caused by the respiratory cycle

The common approach to the problem of respiratory blurring of PET images is respiratory gating [67] (discussed later); however, two exceptions can be mentioned.

Respiratory-correlated dynamic imaging

In the work by Nehmeh and colleagues [68], a method performing respiratory phase isolation while not making use of gating was implemented (in lung cancer imaging). A radioactive point source was set on the patient's abdomen, and the data were acquired in very short (eg, 1-second) consecutive time frames and individually reconstructed. To capture a specific phase within the breathing cycle, all images were analyzed, and those with the point source at a specific (user-selected) position were identified, with the corresponding sinograms summed and reconstructed using iterative reconstruction.

Compared with respiratory gating, this method, although involving significantly more computation, has the following advantages: (1) it does not require tracking hardware to monitor and trace respiratory motion (a benefit for small institutions that do not have a gating system); (2) it allows reconstruction of PET images at any breathing phase (eg, phase-matching with the CT image data acquired on PET/CT scanners); and (3) it is less susceptible to irregular breathing and allows the exclusion of data from irregular breathing cycles. Similar to the conventional gating approach, however, it has the disadvantage of less data being used in each reconstruction, resulting in noisier images. A closely related respiratory-correlated 4D anatomic and functional information technique acquires the breathing cycle by using a thermometer in the patient's breathing airflow inserted into the

entry of an "oxygen mask" covering mouth and nose [69].

Nongated motion estimation and reconstruction

Another alternative to gating is the method proposed by Reyes and colleagues [21]. In this approach, a measured respiratory motion model is adapted to each patient's anatomy through affine registrations. The resulting estimated motion is incorporated into the system matrix of the EM algorithm. Compared with the previous method, this approach has the advantage of making use of the entire data for the reconstructions (although not making use of additional hardware). Nevertheless, the robustness of the method needs further investigation, given especially the presence of irregular respiratory patterns and interpatient respiratory variations.

Otherwise, the most common approach is implementation of respiratory gating. For instance, respiratory-gated PET has been investigated in imaging of lung cancer to reduce breathing motion artifacts [53,68,70–76]. In cardiac imaging, combined cardiac–respiratory gating has been implemented in human [41,42,77] and animal [39,40] studies.

Instrumentation

A number of instruments are used for measuring respiratory motion [67,78]. Commonly, a pneumatic bellows is placed around the midabdomen of the patient, which monitors variation in pressure in the belt assembly with stretching of the belt during respiration [41,79]. The Anzai AZ-733V system (Anzai Medical Co, Ltd., Tokyo, Japan), which uses a pressure sensor to measure the expansion of the chest, thus detecting the external respiratory motion (pressure change) in real time, has been used by many investigators [42,74].

Another approach involves the real-time position management respiratory gating system (Varian Medical Systems, Palo Alto, California) [68,71,80], which monitors the motion of the chest wall of the patient by IR tracking of the vertical position of two reflective markers mounted on a plastic block (stabilized on the patient's abdomen). The system was further refined more recently to enable the analysis of the marker block motion in all three dimensions as it moves up and down, forward and back, and side to side.

Livieratos and colleagues [81] used an inductive respiration monitor (RespiTrace R250, Studley Data Systems, Oxford, UK) with an elasticized belt around the patient's chest.

In animal (mice) imaging, a respiration sensor (Graseby Medical Ltd., Watford, UK) was used by Yang and colleagues [39] to provide the respiratory signal. The sensor was taped to the animal's chest and connected to a high-sensitivity differential pressure transducer.

Beach and colleagues [79] used the POLARIS system (described earlier) during cardiac imaging, which has the advantage of monitoring respiratory and other unwanted motions. Four IR reflective markers placed on an elastic-material band are set around the patient's mid to lower abdomen. The investigators refined the methodology using a neural network approach to decompose monitored patient motion data into rigid body motion and respiratory motion, thus allowing the successful correction for respiratory and rigid body motion using approaches suitable for each type of motion [82].

Finally, Bruyant and colleagues [83] devised a robust approach for tracking and compensating patient motion by combining an emission data–based approach with a visual tracking system that provides an independent estimate of motion. The visual tracking system includes stereo imaging with sets of optical network cameras with attached light sources, a calibration phantom (consisting of seven reflective spheres), a black stretchable garment with reflective spheres to track chest motion, and a computer to control the cameras in synchronization with the list-mode SPECT data acquisition.

Many respiratory tracking systems developed explicitly for radiation therapy applications [78] could be used for imaging purposes. One such example is a robotic respiratory tracking system [84]. Further translational research is required in this area to automate the acquisition/processing procedures required for accurate motion compensation in connection with image-guided radiation therapy.

Respiratory motion-correction algorithm

It should be noted that most of the methods for cardiac motion correction mentioned in the previous section are also applicable to advanced respiratory imaging, assuming that effective respiratory motion estimation methods are developed. In particular, Li and colleagues [19] extracted motion information by adopting the free-form spline model (B-spline) [85] to register different phases of the CT images, and used this information in a truly 4D reconstruction approach (see Category 2 in the section Motion-Correction Algorithms) to obtain improved images in terms of spatial resolution and statistical properties. Examples of this approach (used in a clinical study with a pancreatic tumor) are shown in Fig. 7 and clearly illustrate its advantages compared with other data collection procedures. The figure illustrates reconstructions obtained using the 3D ungated PET obtained by summing the acquired 4D PET projections in group, the conventional 4D gated PET, and the model-based 4D PET algorithm

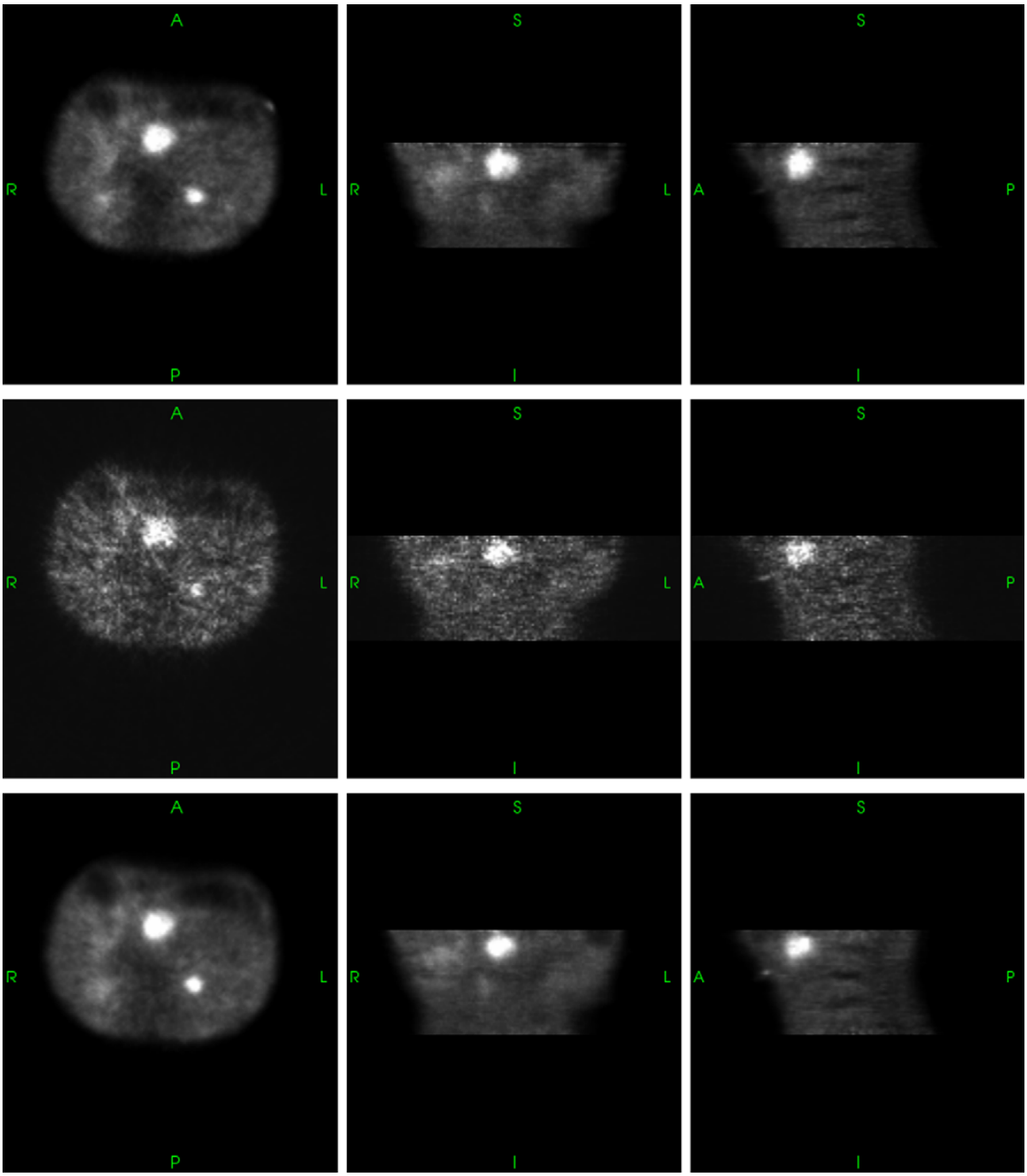

Fig. 7. Reconstructed images of 3D ungated PET obtained by summing all the acquired 4D-PET projections (*top row*), conventional gated 4D PET (*middle row*), and model-based 4D PET (*bottom row*) for a clinical study with pancreatic tumor. (*From* Li T, Thorndyke B, Schreibmann E, et al. Model-based image reconstruction for four-dimensional PET. Med Phys 2006;33:1296; with permission.)

referenced earlier. It can be seen that the tumor is better defined using the model-based 4D PET reconstruction algorithm compared with the conventional 4D gated PET because of the better statistical properties of the data. The SNRs were 2.21, 1.83, and 4.17 for the 3D ungated PET, regular 4D gated PET, and model-based 4D PET, respectively.

Imaging of the heart

In addition to the potential application of the aforementioned general methods to cardiac and respiratory motion correction, there are two respiratory-dedicated methods for the imaging of the heart (the first is implemented in projection-space and the second in image-space) that similarly seek to obtain images of higher quality compared with regular respiratory-gating or respiratory-correlated dynamic imaging.

The work by Livieratos and colleagues [81] performs cardiac imaging by modeling of the respiratory motion of the heart as a rigid-body motion. The motion correction parameters are obtained

from an initial series of respiration-only gated images by way of edge tracking of the left ventricle [43]. The obtained model is then applied in the form of rigid-body transformations (ie, translations and rotations) to the list-mode data event- by- event (ie, motion correction in projection-space). The list-mode approach allows one to make maximal use of the time resolution of list-mode data for interpolation of motion parameters, thus potentially achieving higher accuracy in respiratory motion compensation. After correction of the data for respiratory motion, these investigators proposed to use simple cardiac gating for the rest of the imaging task; however, the authors note that the more advanced methods presented in the previous section can be used instead.

Klein and colleagues [86] investigated a 12-parameter affine motion model for 4D registration of different respiratory-gated images, which in addition to the 6 parameters of rotation and translation allows for 3 scale and 3 skew parameters for nonrigid motion. This approach, which was based in the image-space, was applied to doubly gated cardiac PET sequences because it required images with high SNR for appropriate registration.

Rigid versus nonrigid modeling of the respiratory motion of the heart

Although the validity of modeling (ie, approximating) respiratory motion of the heart as rigid-body motion has been claimed [81], a number of other publications suggest that nonrigid modeling of respiratory motion of the heart may be beneficial. The authors note that the nonrigidity of respiratory motion of the heart, which is related to it being pushed and pulled by the diaphragm and other connected tissue, has been investigated using a number of modalities. For instance, the gated CT study by Hoffman and Ritman [87] measured on dogs recorded an average change of 12% in the total end-diastolic heart volume during forced positive pressure inspiration at 15 cm H_2O. Using echocardiography, similar shape changes have been found in human subjects [88].

Related work by Klein and colleagues [86] in PET imaging is particularly worth noting. In that work, quantitative measures of respiratory motion of the heart were extracted from 10 respiratory-gated patient studies. Translations between end-inspiration and end-expiration were often greater than 10 mm and ranged from 1 mm to over 20 mm (rigid motion). Moreover, the left ventricle exhibited large compression factors[5] (nonrigid motion)—close to 10% in a number of cases—computed as the product of the three extension factors along the x, y, and z directions.

The extension factors were largest along the superior/inferior axis ($\sim$5%), which given the typical 80- to 100-mm dimension of the left ventricle along this direction, would result in a heart image that would be 4 to 5 mm too small if motion was assumed to be simply rigid. Compared with the average 10-mm thickness of the left ventricular wall, this scaling error may therefore be considerable. With a high-resolution scanner, however, only small improvements were actually observed [86] after performing nonrigid motion modeling, although it is expected that in next-generation (higher-resolution) scanners, further improvements may be observed.

Respiratory-gated imaging of the lung

The two methods mentioned in the Imaging of the Heart section (based on rigid or non-rigid, 4D affine–transformed modeling of respiratory motion of the heart) are hardly applicable to imaging of the lungs, which have a more complicated motion. In the method proposed by Ue and colleagues [89], an objective function consisting of (1) the degree of similarity between a reference image and a deformed image and (2) the smoothness of deformation is identified and optimized using a simulated annealing algorithm. An expansion ratio (defined as the ratio of change in local volume due to deformation) is introduced in the degree of similarity term of the objective function to preserve the total activity during the motion correction process. The algorithm allowed to achieve acceptable motion correction between inspiration and expiration phase images in phantom and clinical data.

The authors emphasize that this approach is a motion estimation method. The particular reconstruction approach of the authors (summing of final images) can be substituted by other methods, as mentioned in the previous section, particularly those that incorporate the estimated motion from gated images inside the reconstruction algorithm (see the section Motion-Correction Algorithms) and that are expected to result in more favorable images (although they are more time-consuming).

Areas of future research

In this section, several areas of research in motion correction that still remain open questions and important areas demanding further inquiries and research are outlined.

[5] The left ventricle was generally largest at inspiration and smallest at end-expiration.

Current motion tracking devices and correction methods in brain imaging do not address the occurrence of relative motions between the skin and the skull during the scans. This can imply an inaccuracy, because motion-tracking lights or reflectors only follow the motion of the surface area to which they are attached (and not necessarily the regions of interest inside the brain). It is currently a topic of growing interest to introduce novel methods of characterizing and correcting for this issue.

Incorporation of accurate coincidental-accidence (random) and scattered-events correction terms considering patient motion has received little attention in the past [22,30,32] because normalization/attenuation correction and LOR transformations have been the major issues. In this regard, it is noted that current random and scatter estimation techniques commonly assume a static patient, and therefore, further attention needs to be paid to this topic [90].

It remains an open task to theoretically analyze and thoroughly compare methods in which cardiac motion and respiratory motion are estimated (1) before the application of an advanced image reconstruction algorithm (that makes use of the estimated motion) or (2) simultaneously with the image reconstruction task [18,21,63,91].

The principal component analysis method elaborated by Wernick and colleagues [92] is a very efficient and natural framework for fast 4D image reconstructions. Although the method was developed for the motion-free object assumption, it has also been shown to work well in reconstructing cardiac image sequences [93] (which can indicate that the method is somehow able to intrinsically capture and incorporate motion information). More work is needed in this area to shed light on the potential of this technique to include accurate motion compensation [61].

Evaluation and clinical validation of algorithms developed to improve image quality is inherently difficult and sometimes unconvincing, particularly when applied to clinical data in the absence of a "gold standard." There is a clear need for guidelines to evaluate image enhancement and analysis techniques and other image processing issues in PET. Different approaches have been suggested to judge image quality when evaluating image correction and reconstruction algorithms. Because the "best" algorithm can only be selected with respect to a certain task, different "basic" performance measures can be used.

One of the most active areas of research and development in radiologic imaging has been the advanced physical anthropomorphic phantoms and computational models that represent the human anatomy [94]. One such computational model is the 4D nonuniform rational B-spline surfaces–based cardiac-torso (NCAT) model developed by Segars [95] that uses mathematical formulae and the size, shape, and configurations of the major thoracic structures and organs such as the heart, liver, breasts, and rib cage to achieve realistic modeling. Incorporation of accurate models of cardiac and respiratory physiology into the current 4D NCAT model was a significant step toward accounting for inherent cardiac and respiratory motion not considered in the previous models. Paganetti [96] reported on the simulation of time-dependent geometries within a single 4D Monte Carlo simulation using the GEANT4 Monte Carlo package.

Likewise, many physical static anthropomorphic phantoms were developed in corporate settings, but very few dynamic torso phantoms are commercially available (and all of these are specifically designed for the assessment of cardiac scanning protocols and ejection fraction calculation software). Many academic investigators have built dynamic physical phantoms to meet their research needs in cardiac imaging [97–99]; however, similar to commercial systems, virtually all of them do not incorporate respiratory motion modeling. More advanced technologies allow the construction of dynamic phantoms allowing modeling of respiratory motion [100]. One interesting design is the platform developed by Fitzpatrick and colleagues [101] that is capable of programmable irregular longitudinal motion (artificially generated on a spreadsheet or extracted from respiratory monitoring files) to simulate intrafractional respiratory motion.

Summary

In this article, the authors review advanced correction methods in PET for the cases of unwanted patient motion and unwanted motion due to cardiac cycles and respiratory cycles. Nearly all the work related to the first type of motion has been in brain PET imaging. The use of an external motion-tracking device (and not solely relying on the emission data) is attractive and will become popular for high-resolution PET imaging in the near future.

In brain PET imaging, given the rigid nature of motion, it is more accurate to perform motion corrections in projection-space than in image-space to make maximal use of the time resolution of data. A number of reviewed works have also observed and proposed solutions to complications caused by the motion-based interactions of LORs that are normally detectable and those that are not (eg, axially out of the FoV or passing through detector gaps).

In advanced cardiac and respiratory correction schemes, the authors have observed a general attempt to move beyond the noisy images obtained

by cardiac- and respiratory-gated data that are individually reconstructed, to advanced techniques that make use of novel motion estimation and image reconstruction applications to obtain images of enhanced quality (improved SNR and resolution). It is observed from the works reviewed in this article that a general theme is the use of increasingly sophisticated software to make use of existing advanced hardware, and that the field of motion correction in high-resolution PET is open to future novel ideas (hardware, and especially software) aimed at improving motion detection, characterization, and compensation.

References

[1] Zaidi H. Recent developments and future trends in nuclear medicine instrumentation. Z Med Phys 2006;16:5–17.

[2] Lopresti BJ, Russo A, Jones WF, et al. Implementation and performance of an optical motion tracking system for high resolution brain PET imaging. IEEE Trans Nucl Sci 1999;46:2059–67.

[3] Herzog H, Tellmann L, Fulton R, et al. Motion artifact reduction on parametric PET images of neuroreceptor binding. J Nucl Med 2005;46: 1059–65.

[4] Zaidi H, Montandon M-L, Meikle S. Strategies for attenuation compensation in neurological PET studies. Neuroimage 2007;34:518–41.

[5] Fulton RR, Meikle SR, Eberl S, et al. Correction for head movements in positron emission tomography using an optical motion-tracking system. IEEE Trans Nucl Sci 2002;49:116–23.

[6] Bloomfield PM, Spinks TJ, Reed J, et al. The design and implementation of a motion correction scheme for neurological PET. Phys Med Biol 2003;48:959–78.

[7] Ruttimann UE, Andreason PJ, Rio D. Head motion during positron emission tomography: is it significant? Psychiatry Res 1995;61:43–51.

[8] Woods RP, Cherry SR, Mazziotta JC. Rapid automated algorithm for aligning and reslicing PET images. J Comput Assist Tomogr 1992;16: 620–33.

[9] Friston KJ, Ashburner J, Frith CD, et al. Spatial registration and normalisation of images. Human Brain Mapp 1995;2:165–89.

[10] Tellmann L, Fulton R, Pietrzyk U, et al. Concepts of registration and correction of head motion in positron emission tomography. Z Med Phys 2006;16:67–74.

[11] Hutton BF, Kyme AZ, Lau YH, et al. A hybrid 3-D reconstruction/registration algorithm for correction of head motion in emission tomography. IEEE Trans Nucl Sci 2002;49:188–94.

[12] Kyme AZ, Hutton BF, Hatton RL, et al. Practical aspects of a data-driven motion correction approach for brain SPECT. IEEE Trans Med Imaging 2003;22:722–9.

[13] Schafers KP, Dawood M, Lang N, et al. Motion correction in PET/CT. Nuklearmedizin 2005; 44(Suppl 1):S46–50.

[14] Picard Y, Thompson CJ. Motion correction of PET images using multiple acquisition frames. IEEE Trans Med Imaging 1997;16:137–44.

[15] Goldstein SR, Daube-Witherspoon ME, Green MV, et al. A head motion measurement system suitable for emission computed tomography. IEEE Trans Med Imaging 1997;16:17–27.

[16] Menke M, Atkins MS, Buckley KR. Compensation methods for head motion detected during PET imaging. IEEE Trans Nucl Sci 1996;43: 310–7.

[17] El Naqa I, Low DA, Bradley JD, et al. Deblurring of breathing motion artifacts in thoracic PET images by deconvolution methods. Med Phys 2006;33:3587–600.

[18] Qiao F, Pan T, Clark JW Jr, et al. A motion-incorporated reconstruction method for gated PET studies. Phys Med Biol 2006;51:3769–83.

[19] Li T, Thorndyke B, Schreibmann E, et al. Model-based image reconstruction for four-dimensional PET. Med Phys 2006;33:1288–98.

[20] Qiao F, Pan T, Clark JW, et al. Region of interest motion compensation for PET image reconstruction. Phys Med Biol 2007;52:2675–89.

[21] Reyes M, Malandain G, Koulibaly PM, et al. Model-based respiratory motion compensation for emission tomography image reconstruction. Phys Med Biol 2007;52:3579–600.

[22] Rahmim A, Cheng JC, Dinelle K, et al. System matrix modeling of externally tracked motion. IEEE Nuclear Science Symposium Conference Record 2006;4:2137–41.

[23] Daube-Witherspoon M, Yan Y, Green M, et al. Correction for motion distortion in PET by dynamic monitoring of patient position [abstract]. J Nucl Med 1990;31:816.

[24] Bühler P, Just U, Will E, et al. An accurate method for correction of head movement in PET. IEEE Trans Med Imaging 2004;23:1176–85.

[25] Jones WF. Real-time event stream correction for patient motion in clinical 3-D PET. IEEE Nuclear Science Symposium Conference Record 2001;4:2062–4.

[26] Qi J, Huesman R. Correction of motion in PET using event-based rebinning method: pitfall and solution [abstract]. J Nucl Med 2002;43: 146P.

[27] Rahmim A, Bloomfield P, Houle S, et al. Motion compensation in histogram-mode and list-mode EM reconstructions: beyond the event-driven approach. IEEE Trans Nucl Sci 2004;51: 2588–96.

[28] Wienhard K, Schmand M, Casey ME, et al. The ECAT HRRT: performance and first clinical application of the new high resolution research tomograph. IEEE Trans Nucl Sci 2002;49: 104–10.

[29] Braem A, Chamizo Llatas M, Chesi E, et al. Feasibility of a novel design of high-resolution

parallax-free Compton enhanced PET scanner dedicated to brain research. Phys Med Biol 2004;49:2547–62.
[30] Thielemans K, Mustafovic S, Schnorr L. Image reconstruction of motion corrected sinograms. IEEE Nuclear Science Symposium Conference Record 2003;4:2401–6.
[31] Qi J, Huesman RH. List mode reconstruction for PET with motion compensation: a simulation study. Proceedings of the IEEE International Symposium on Biomedical Imaging 2002;413–6.
[32] Rahmim A, Dinelle K, Cheng J, et al. Accurate event-driven motion compensation in high-resolution PET incorporating scattered and random events. IEEE Trans Med Imaging, in press.
[33] Rahmim A, Lenox M, Reader AJ, et al. Statistical list-mode image reconstruction for the high resolution research tomograph. Phys Med Biol 2004;49:4239–58.
[34] Rahmim A, Cheng J-C, Blinder S, et al. Statistical dynamic image reconstruction in state-of-the-art high-resolution PET. Phys Med Biol 2005;50:4887–912.
[35] Carson RE, Barker WC, Liow J-S, et al. Design of a motion-compensation OSEM list-mode algorithm for resolution-recovery reconstruction for the HRRT. IEEE Nuclear Science Symposium Conference Record 2003;5:3281–5.
[36] Qi J, Huesman RH. Propagation of errors from the sensitivity image in list mode reconstruction. IEEE Trans Med Imaging 2004;23:1094–9.
[37] Qi J. Calculation of the sensitivity image in list-mode reconstruction for PET. IEEE Trans Nucl Sci 2006;53:2746–51.
[38] O'Dell WG, Moore CC, Hunter WC, et al. Three-dimensional myocardial deformations: calculation with displacement field fitting to tagged MR images. Radiology 1995;195:829–35.
[39] Yang Y, Rendig S, Siegel S, et al. Cardiac PET imaging in mice with simultaneous cardiac and respiratory gating. Phys Med Biol 2005;50: 2979–89.
[40] Schafers KP, Lang N, Stegger L, et al. Gated list-mode acquisition with the QuadHIDAC animal PET to image mouse hearts. Z Med Phys 2006; 16:60–6.
[41] Lang N, Dawood M, Büther F, et al. Organ movement reduction in PET/CT using dual-gated listmode acquisition. Z Med Phys 2006; 16:93–100.
[42] Martinez-Möller A, Zikic D, Botnar RM, et al. Dual cardiac/respiratory gated PET: implementation and results from a feasibility study. Eur J Nucl Med Mol Imaging 2007;31:1447–54.
[43] Stegger L, Biedenstein S, Schafers KP, et al. Elastic surface contour detection for the measurement of ejection fraction in myocardial perfusion SPET. Eur J Nucl Med 2001;28:48–55.
[44] Naum A, Laaksonen MS, Tuunanen H, et al. Motion detection and correction for dynamic (15)O-water myocardial perfusion PET studies. Eur J Nucl Med Mol Imaging 2005;32: 1378–83.
[45] Di Carli MF, Dorbala S, Meserve J, et al. Clinical myocardial perfusion PET/CT. J Nucl Med 2007; 48:783–93.
[46] Hutchins GD, Caraher JM, Raylman RR. A region of interest strategy for minimizing resolution distortions in quantitative myocardial PET studies. J Nucl Med 1992;33:1243–50.
[47] Nichols K, Lefkowitz D, Faber T, et al. Echocardiographic validation of gated SPECT ventricular function measurements. J Nucl Med 2000; 41:1308–14.
[48] Fitzpatrick GM, Wells RG. Simulation study of respiratory-induced errors in cardiac positron emission tomography/computed tomography. Med Phys 2006;33:2888–95.
[49] Le Meunier L, Maass-Moreno R, Carrasquillo JA, et al. PET/CT imaging: effect of respiratory motion on apparent myocardial uptake. J Nucl Cardiol 2006;13:821–30.
[50] Asma E, Manjeshwar R, Thielemans K. Theoretical comparison of motion correction techniques for PET image reconstruction. IEEE Nuclear Science Symposium Conference Record 2006;3:1762–7.
[51] Klein GJ, Huesman RH. Four-dimensional processing of deformable cardiac PET data. Med Image Anal 2002;6:29–46.
[52] Dawood M, Buther F, Lang N, et al. Transforming static CT in gated PET/CT studies to multiple respiratory phases. Presented at the 18th International Conference on Pattern Recognition. 1:1026–29.
[53] Thorndyke B, Schreibmann E, Koong A, et al. Reducing respiratory motion artifacts in positron emission tomography through retrospective stacking. Med Phys 2006;33:2632–41.
[54] Brankov JG, Yang Y, Narayanan MV, et al. Motion-compensated 4D processing of gated SPECT perfusion studies. IEEE Nuclear Science Symposium Conference Record 2002;3:1380–4.
[55] Brankov JG, Yang Y, Feng B, et al. 4D smoothing of gated SPECT images using a left-ventricle shape model and a deformable mesh. IEEE Nuclear Science Symposium Conference Record 2004;5:2845–8.
[56] Lamare F, Cresson T, Savean J, et al. Respiratory motion correction for PET oncology applications using affine transformation of list mode data. Phys Med Biol 2007;52:121–40.
[57] Geman S, McClure D. Bayesian image analysis: an application to single photon emission tomography. Proceedings of the American Statistical Society, Statistical Computing Section. Washington, DC, 2006:12–18.
[58] Green PJ. Bayesian reconstructions from emission tomography data using a modified EM algorithm. IEEE Trans Med Imaging 1990;9: 84–93.
[59] Lalush DS, Lin C, Tsui BMW. A priori motion models for four-dimensional reconstruction in

gated cardiac SPECT. IEEE Nuclear Science Symposium Conference Record 1996;3:1923–7.
[60] Gravier EJ, Yang Y. Motion-compensated reconstruction of tomographic image sequences. IEEE Trans Nucl Sci 2005;52:51–6.
[61] Gravier E, Yang Y, King MA, et al. Fully 4D motion-compensated reconstruction of cardiac SPECT images. Phys Med Biol 2006;51:4603–19.
[62] Horn B, Schunck B. Determining optical flow. Artificial Intelligence 1981;17:185–203.
[63] Cao Z, Gilland DR, Mair BA, et al. Three-dimensional motion estimation with image reconstruction for gated cardiac ECT. IEEE Trans Nucl Sci 2003;50:384–8.
[64] Gilland DR, Mair BA, Sun J. Joint 4D reconstruction and motion estimation in gated cardiac ECT. Proceedings of the International Meeting on Fully Three-Dimensional Image Reconstruction in Radiology and Nuclear Medicine. Salt Lake City, July 6–9, 2005.
[65] Jacobson MW, Fessler JA. Joint estimation of image and deformation parameters in motion-corrected PET. IEEE Nuclear Science Symposium Conference Record 2003;5:3290–4.
[66] Jacobson MW, Fessler JA. Joint estimation of respiratory motion and activity in 4D PET using CT side information. Presented at the 3rd IEEE International Symposium on Biomedical Imaging: Nano to Macro. Arlington, VA, April 6–9, 2006.
[67] Visvikis D, Lamare F, Bruyant P, et al. Respiratory motion in positron emission tomography for oncology applications: problems and solutions. Nuclear Instruments and Methods in Physics Research Section A 2006;569:453–7.
[68] Nehmeh SA, Erdi YE, Rosenzweig KE, et al. Reduction of respiratory motion artifacts in PET imaging of lung cancer by respiratory correlated dynamic PET: methodology and comparison with respiratory gated PET. J Nucl Med 2003; 44:1644–8.
[69] Wolthaus JW, van Herk M, Muller SH, et al. Fusion of respiration-correlated PET and CT scans: correlated lung tumour motion in anatomical and functional scans. Phys Med Biol 2005;50: 1569–83.
[70] Boucher L, Rodrigue S, Lecomte R, et al. Respiratory gating for 3-dimensional PET of the thorax: feasibility and initial results. J Nucl Med 2004;45:214–9.
[71] Nehmeh SA, Erdi YE, Pan T, et al. Quantitation of respiratory motion during 4D-PET/CT acquisition. Med Phys 2004;31:1333–8.
[72] Erdi YE, Nehmeh SA, Pan T, et al. The CT motion quantitation of lung lesions and its impact on PET-measured SUVs. J Nucl Med 2004;45: 1287–92.
[73] Dawood M, Lang N, Jiang X, et al. Lung motion correction on respiratory gated 3-D PET/CT images. IEEE Trans Med Imaging 2006;25:476–85.
[74] Bundschuh RA, Martinez-Moeller A, Essler M, et al. Postacquisition detection of tumor motion in the lung and upper abdomen using list-mode PET data: a feasibility study. J Nucl Med 2007;48:758–63.
[75] Nehmeh SA, Erdi YE, Meirelles GS, et al. Deep-inspiration breath-hold PET/CT of the thorax. J Nucl Med 2007;48:22–6.
[76] Dawood M, Buther F, Lang N, et al. Respiratory gating in positron emission tomography: a quantitative comparison of different gating schemes. Med Phys 2007;34:3067–76.
[77] Klein GJ, Reutter BW, Ho MH, et al. Real-time system for respiratory-cardiac gating in positron tomography. IEEE Trans Nucl Sci 1998;45: 2139–43.
[78] Keall PJ, Mageras GS, Balter JM, et al. The management of respiratory motion in radiation oncology—report of AAPM Task Group 76. Med Phys 2006;33:3874–900.
[79] Beach RD, Pretorius PH, Boening G, et al. Feasibility of stereo-infrared tracking to monitor patient motion during cardiac SPECT imaging. IEEE Trans Nucl Sci 2004;51:2693–8.
[80] Vedam SS, Keall PJ, Kini VR, et al. Acquiring a four-dimensional computed tomography dataset using an external respiratory signal. Phys Med Biol 2003;48:45–62.
[81] Livieratos L, Stegger L, Bloomfield PM, et al. Rigid-body transformation of list-mode projection data for respiratory motion correction in cardiac PET. Phys Med Biol 2005;50:3313–22.
[82] Beach RD, Depold H, Boening G, et al. An adaptive approach to decomposing patient-motion tracking data acquired during cardiac SPECT imaging. IEEE Trans Nucl Sci 2007;54: 130–9.
[83] Bruyant PP, Gennert MA, Speckert GC, et al. A robust visual tracking system for patient motion detection in SPECT: hardware solutions. IEEE Trans Nucl Sci 2005;52:1288–94.
[84] Seppenwoolde Y, Berbeco RI, Nishioka S, et al. Accuracy of tumor motion compensation algorithm from a robotic respiratory tracking system: a simulation study. Med Phys 2007;34:2774–84.
[85] Mattes D, Haynor DR, Vesselle H, et al. PET-CT image registration in the chest using free-form deformations. IEEE Trans Med Imaging 2003; 22:120–8.
[86] Klein GJ, Reutter RW, Huesman RH. Four-dimensional affine registration models for respiratory-gated PET. IEEE Trans Nucl Sci 2001;48: 756–60.
[87] Hoffman EA, Ritman EL. Heart-lung interaction: effect on regional lung air content and total heart volume. Ann Biomed Eng 1987;15: 241–57.
[88] Andersen K, Vik-Mo H. Effects of spontaneous respiration on left ventricular function assessed by echocardiography. Circulation 1984;69: 874–9.
[89] Ue H, Haneishi H, Iwanaga H, et al. Nonlinear motion correction of respiratory-gated lung SPECT images. IEEE Trans Med Imaging 2006; 25:486–95.

[90] Zaidi H, Koral KF. Scatter modelling and compensation in emission tomography. Eur J Nucl Med Mol Imaging 2004;31:761–82.
[91] Feng B, Gifford HC, Beach RD, et al. Use of three-dimensional Gaussian interpolation in the projector/backprojector pair of iterative reconstruction for compensation of known rigid-body motion in SPECT. IEEE Trans Med Imaging 2006;25:838–44.
[92] Wernick MN, Infusino EJ, Milosevic M. Fast spatio-temporal image reconstruction for dynamic PET. IEEE Trans Med Imaging 1999;18: 185–95.
[93] Narayanan MV, King MA, Soares EJ, et al. Application of the Karhunen-Loeve transform to 4D reconstruction of cardiac gated SPECT images. IEEE Trans Nucl Sci 1999;46:1001–8.
[94] Zaidi H, Xu XG. Computational anthropomorphic models of the human anatomy: the path to realistic Monte Carlo modeling in medical imaging. Annu Rev Biomed Eng 2007;9: 471–500.
[95] Segars WP. Development and application of the new dynamic NURBS-based cardiac-torso (NCAT) phantom [PhD Thesis]. Chapel Hill (NC): University of North Carolina; 2001.
[96] Paganetti H. Four-dimensional Monte Carlo simulation of time-dependent geometries. Phys Med Biol 2004;49:N75–81.
[97] De Bondt P, Claessens T, Rys B, et al. Accuracy of 4 different algorithms for the analysis of tomographic radionuclide ventriculography using a physical, dynamic 4-chamber cardiac phantom. J Nucl Med 2005;46:165–71.
[98] Begemann PG, van Stevendaal U, Manzke R, et al. Evaluation of spatial and temporal resolution for ECG-gated 16-row multidetector CT using a dynamic cardiac phantom. Eur Radiol 2005;15:1015–26.
[99] Al Hamwi A. [Construction and optimal design of a dynamic heart phantom for simulation of motion artifacts in PET scan]. Biomed Tech (Berl) 2002;47(Suppl 1 Pt 2):810–1 [in German].
[100] Kashani R, Hub M, Kessler ML, et al. Technical note: a physical phantom for assessment of accuracy of deformable alignment algorithms. Med Phys 2007;34:2785–8.
[101] Fitzpatrick MJ, Starkschall G, Balter P, et al. A novel platform simulating irregular motion to enhance assessment of respiration-correlated radiation therapy procedures. J Appl Clin Med Phys 2005;6:13–21.